Near-Field Sensing and Communications with Reconfigurable Antennas

Xianghao Yu

Assistant Professor
Department of Electrical Engineering
City University of Hong Kong
Hong Kong SAR

December 3rd, 2025

香港城市大學
City University of Hong Kong
NSFC
National Natural Science Foundation of China
UGC 大學教育資助委員會
University Grants Committee
IEEE ComSoc
IEEE

Outline

Outline

Introduction

- Every leap in wireless systems from 2G to 5G has been propelled by relentless advancements in antenna technology

(a)

(b)

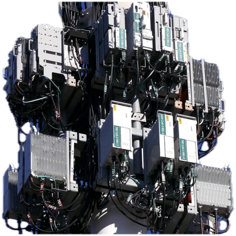

(c)

Figure 1: (a) Omnidirectional single antenna, (b) Sectored array, (c) Multi-beam station

Introduction

- **XL-MIMO** antenna arrays widely investigated in beyond 5G systems

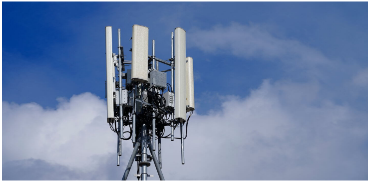

(a) Massive MIMO BS

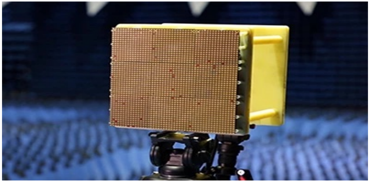

(b) Recofigurable Intelligent Surface

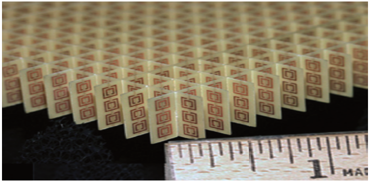

(c) Holographic MIMO

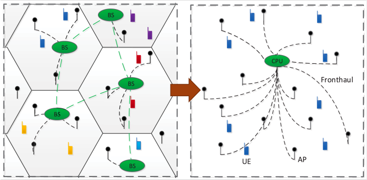

(d) Cell-free mMIMO

Figure 2: Widely investigated XL-MIMO related topics.

Introduction

- **XL-MIMO** with large aperture and massive elements **expands the near-field (NF) region**
- Near-field region, a.k.a., Fresnel region, is bounded as

$$\sqrt[3]{\frac{2D^4}{\boldsymbol{\lambda}}} \leq d_{\mathrm{NF}} \leq \frac{2D^2}{\boldsymbol{\lambda}}, \qquad D\blacktriangle \;\; \boldsymbol{\lambda}\blacktriangledown \Rightarrow d_{\mathrm{NF}}\blacktriangle$$

- A 50 m distance already falls in the NF region of a 64-element array operating at centimetre wave $f_c = 10$ GHz

Introduction

- Near-field region, a.k.a., Fresnel region, expands significantly

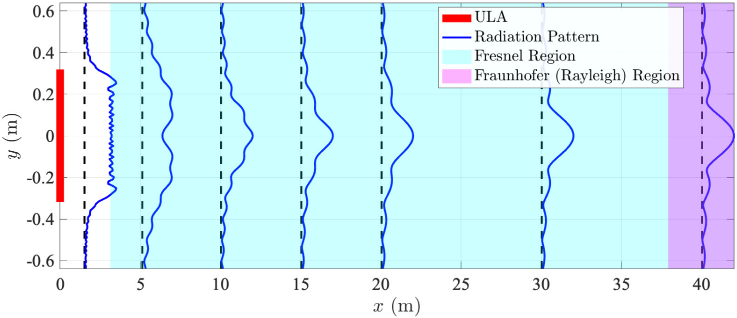

Figure 3: Radiation Pattern at different distances.

- Determined not only by **Angle θ** but also by **Distance r**

Introduction

- In the **near-field** region, EM wavefront is not planar, but **spherical**

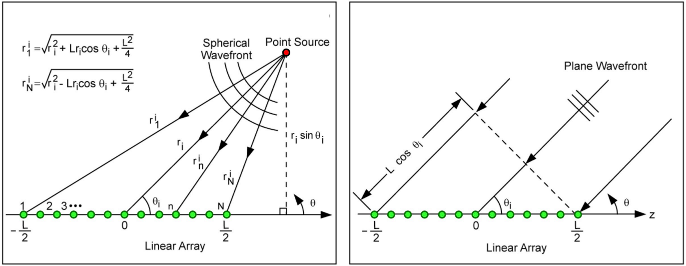

Figure 4: Wavefront illustration [1].

- Spatial (channel) response:

$$g\left(\mathbf{r}_{\mathrm{BS}}^{(n)}, \mathbf{r}_{\mathrm{UE}}^{(m)}\right) = e^{-\jmath\kappa\sqrt{\left\|\mathbf{r}_{\mathrm{BS}}^{(n)}\right\|^2 + \left\|\mathbf{r}_{\mathrm{UE}}^{(m)}\right\|^2 - 2\left\|\mathbf{r}_{\mathrm{BS}}^{(n)}\right\|\left\|\mathbf{r}_{\mathrm{UE}}^{(m)}\right\|\cos(\vartheta_{m,n})}}$$

[1] A. Fenn, "Evaluation of adaptive phased array antenna, far-field nulling performance in the near-field region," *IEEE Trans. Antennas Propag.*, vol. 38, no. 2, pp. 173–185, 1990.

Challenges in Near-Field Sensing & Communications

- Two degrees of freedoms (r, θ) in NF channels
- Sensing/channel estimation
  - More parameters to be estimated
  - A large number of **high-speed ADCs** for baseband sampling
  - Polynomially increasing **computational complexity**

Challenges in Near-Field Sensing & Communications

- Two degrees of freedoms (r, θ) in NF channels
- Sensing/channel estimation
  - More parameters to be estimated
  - A large number of **high-speed ADCs** for baseband sampling
  - Polynomially increasing **computational complexity**
- Communications
  - Conventional **uniform** array geometry cannot effectively capture the **non-uniform** spatial variation in the NF spherical wavefront
  - Lack of **customized** design methodologies for NF communications

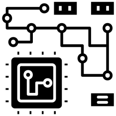

Hardware

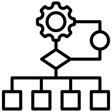

Algorithm

Outline

Outline

Power Sensor-Enabled Localization: Recording

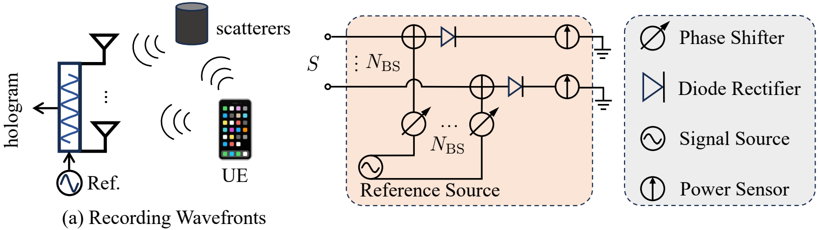

- Received signal at the n-th antenna element of the BS, $\mathbf{e}_{\mathrm{obj}}[n]$, carrying the NF channel information $g\left(\mathbf{r}_{\mathrm{BS}}^{(n)}, \mathbf{r}_{\mathrm{UE}}\right)$
- Antennas elements record the power

$$\begin{aligned}\mathbf{p}[n] &= \left|\mathbf{e}_{\mathrm{ref}}[n] + \mathbf{e}_{\mathrm{obj}}[n]\right|^2 \\ &= \left|\mathbf{e}_{\mathrm{ref}}[n]\right|^2 + \left|\mathbf{e}_{\mathrm{obj}}[n]\right|^2 + \underbrace{\mathbf{e}_{\mathrm{ref}}^*[n]\mathbf{e}_{\mathrm{obj}}[n]}_{\text{Desired}} + \mathbf{e}_{\mathrm{ref}}[n]\mathbf{e}_{\mathrm{obj}}^*[n],\end{aligned}$$

Power Sensor-Enabled Localization: Recording

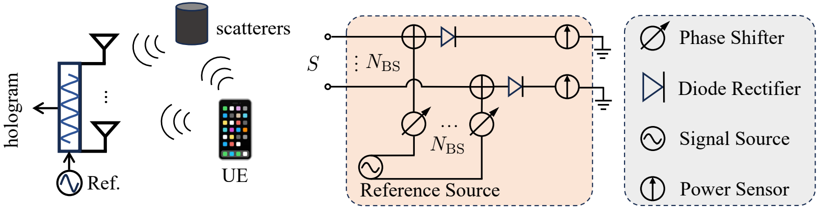

(a) Recording Wavefronts

- Received signal at the n-th antenna element of the BS, $\mathbf{e}_{\mathrm{obj}}[n]$, carrying the NF channel information $g\left(\mathbf{r}_{\mathrm{BS}}^{(n)}, \mathbf{r}_{\mathrm{UE}}\right)$
- Antennas elements record the power

$$\begin{aligned}\mathbf{p}[n] &= \left|\mathbf{e}_{\mathrm{ref}}[n] + \mathbf{e}_{\mathrm{obj}}[n]\right|^2 \\ &= \left|\mathbf{e}_{\mathrm{ref}}[n]\right|^2 + \left|\mathbf{e}_{\mathrm{obj}}[n]\right|^2 + \underbrace{\mathbf{e}_{\mathrm{ref}}^*[n]\mathbf{e}_{\mathrm{obj}}[n]}_{\text{Desired}} + \mathbf{e}_{\mathrm{ref}}[n]\mathbf{e}_{\mathrm{obj}}^*[n],\end{aligned}$$

Power Sensor-Enabled Localization: Reconstruction I

- Remove the undesired signals, build **hologram**

$$\mathbf{p}[n] - |\mathbf{e}_{\text{ref}}[n]|^2 \gtrsim \underbrace{\mathbf{e}_{\text{ref}}^*[n]\mathbf{e}_{\text{obj}}[n]}_{\text{Desired}} + \mathbf{e}_{\text{ref}}[n]\mathbf{e}_{\text{obj}}^*[n]$$
$$\triangleq \boldsymbol{\hbar}[n],$$

- Recover the phase information of $\mathbf{e}_{\text{obj}}[n]$

$$\overline{\boldsymbol{\hbar}}[n] = \boldsymbol{\hbar}[n]\mathbf{e}_{\text{ref}}[n]$$

- Construct a field $\tilde{E}(\mathbf{r})$ by emulating Back-Projection of EM wave from BS to any location $\mathbf{r}$

$$\tilde{E}(\mathbf{r}) = \sum_{n=1}^{N_{\text{BS}}} \overline{\boldsymbol{\hbar}}[n] \|\mathbf{r} - \mathbf{r}_{\text{BS}}^{(n)}\| g^* \left(\mathbf{r}_{\text{BS}}^{(n)}, \mathbf{r}\right)$$

Power Sensor-Enabled Localization: Reconstruction I

- Remove the undesired signals, build **hologram**

$$\mathbf{p}[n] - |\mathbf{e}_{\text{ref}}[n]|^2 \gtrsim \underbrace{\mathbf{e}^*_{\text{ref}}[n]\mathbf{e}_{\text{obj}}[n]}_{\text{Desired}} + \mathbf{e}_{\text{ref}}[n]\mathbf{e}^*_{\text{obj}}[n]$$

$$\triangleq \boldsymbol{\hbar}[n],$$

- Recover the phase information of $\mathbf{e}_{\text{obj}}[n]$

$$\overline{\boldsymbol{\hbar}}[n] = \boldsymbol{\hbar}[n]\mathbf{e}_{\text{ref}}[n]$$

- Construct a field $\tilde{E}(\mathbf{r})$ by emulating Back-Projection of EM wave from BS to any location $\mathbf{r}$

$$\tilde{E}(\mathbf{r}) = \sum_{n=1}^{N_{\text{BS}}} \overline{\boldsymbol{\hbar}}[n] \|\mathbf{r} - \mathbf{r}_{\text{BS}}^{(n)}\| g^* \left(\mathbf{r}_{\text{BS}}^{(n)}, \mathbf{r}\right)$$

Power Sensor-Enabled Localization: Reconstruction I

- Remove the undesired signals, build **hologram**

$$\mathbf{p}[n] - |\mathbf{e}_{\mathrm{ref}}[n]|^2 \gtrsim \underbrace{\mathbf{e}^*_{\mathrm{ref}}[n]\mathbf{e}_{\mathrm{obj}}[n]}_{\text{Desired}} + \mathbf{e}_{\mathrm{ref}}[n]\mathbf{e}^*_{\mathrm{obj}}[n]$$
$$\triangleq \boldsymbol{\hbar}[n],$$

- Recover the phase information of $\mathbf{e}_{\mathrm{obj}}[n]$

$$\overline{\boldsymbol{\hbar}}[n] = \boldsymbol{\hbar}[n]\mathbf{e}_{\mathrm{ref}}[n]$$

- Construct a field $\tilde{E}(\mathbf{r})$ by emulating Back-Projection of EM wave from BS to any location $\mathbf{r}$

$$\tilde{E}(\mathbf{r}) = \sum_{n=1}^{N_{\mathrm{BS}}} \overline{\boldsymbol{\hbar}}[n] \|\mathbf{r} - \mathbf{r}^{(n)}_{\mathrm{BS}}\| g^* \left(\mathbf{r}^{(n)}_{\mathrm{BS}}, \mathbf{r}\right)$$

Power Sensor-Enabled Localization: Reconstruction II

- **Back projection/Time inversion** localization algorithm

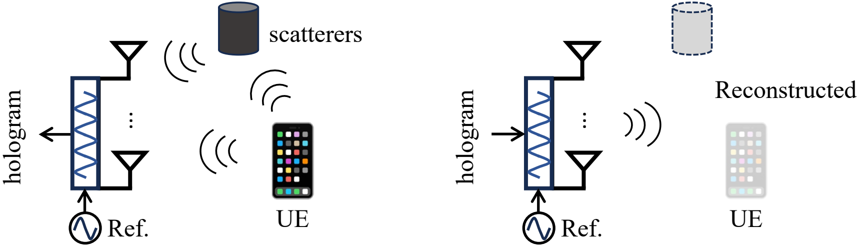

(a) Recording Wavefronts (b) **Emulate** Wavefront Back-projection

- $\mathbf{e}_{\mathrm{obj}}[n]$: Generated by the **forward** propagation $g\left(\mathbf{r}_{\mathrm{BS}}^{(n)}, \mathbf{r}\right)$
- $\tilde{E}(\mathbf{r})$: **Back-project** the processed $\mathbf{e}_{\mathrm{obj}}[n]$ via $g^*\left(\mathbf{r}_{\mathrm{BS}}^{(n)}, \mathbf{r}\right)$

Power Sensor-Enabled Localization: Reconstruction III

- The reconstructed object wave consists of THREE parts

$$\tilde{E}(\mathbf{r}) = \sum_{n=1}^{N_{\mathrm{BS}}} \left(\underbrace{\left|\mathbf{e}_{\mathrm{ref}}[n]\right|^2 \overline{\mathbf{e}}_{\mathrm{obj}}[n] g^* \left(\mathbf{r}_{\mathrm{BS}}^{(n)}, \mathbf{r}\right)}_{\text{desired}} + \underbrace{\left(\mathbf{e}_{\mathrm{ref}}[n]\right)^2 \overline{\mathbf{e}}_{\mathrm{obj}}^*[n] g^* \left(\mathbf{r}_{\mathrm{BS}}^{(n)}, \mathbf{r}\right)}_{\text{interference}} \right)$$

$$= A^2 \sum_{\ell=0}^{L} \overline{\alpha}_\ell \left(\tilde{E}_\ell^{\mathrm{d}}(\mathbf{r}) + \tilde{E}_\ell^{\mathrm{i}}(\mathbf{r}) \right) + \tilde{E}^{\mathrm{n}}(\mathbf{r}),$$

namely, the **desired**, the **interference**, and the noise-related terms.

Analysis

Proposition

As the wavenumber $\kappa \to \infty$ and the number of antennas at BS side $N_{\mathrm{BS}} \to \infty$,

$$\lim_{\substack{\kappa\to\infty \\ N_{\mathrm{BS}}\to\infty}} \left|\tilde{E}_\ell^{\mathrm{d}}(\mathbf{r})\right| = \begin{cases} \sum_{n=1}^{N_{\mathrm{BS}}} \frac{1}{d^{(\ell,n)}} & \text{if } \mathbf{r} = \mathbf{r}_{\mathrm{S}}^{(\ell)}, \\ 0 & \text{otherwise,} \end{cases}$$

$$\lim_{\substack{\kappa\to\infty \\ N_{\mathrm{BS}}\to\infty}} \left|\tilde{E}_\ell^{\mathrm{i}}(\mathbf{r})\right| = 0,$$

$$\lim_{N_{\mathrm{BS}}\to\infty} \left|\tilde{E}^{\mathrm{n}}(\mathbf{r})\right| = 0.$$

- $\tilde{E}(\mathbf{r})$ exhibits peaks at locations of UE and scatterers while diminishing to 0 everywhere else

Reconstruction Demo on Meshgrid

- Reconstruction example for one UE and three scatterers.

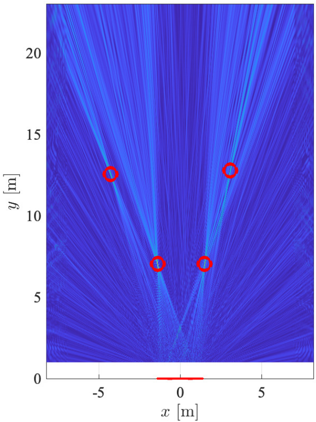

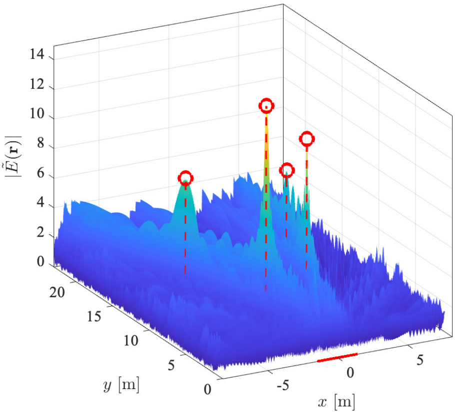

Accelerate Reconstruction via FFT

- Enumerating $\tilde{E}\left(\mathbf{r}^{(i,j)}\right)$ at all possible locations can be computationally heavy
- Reconstruction formula at the (i,j) grid

$$\tilde{E}\left(\mathbf{r}^{(i,j)}\right) = \sum_{n=1}^{N_{\mathrm{BS}}} \boldsymbol{\hbar}[n]\mathbf{e}_{\mathrm{ref}}[n] \quad e^{\jmath\kappa\sqrt{\left(x_{\mathrm{BS}}^{(n)}-x_i\right)^2+y_j^2}}. \tag{1}$$

- Let

$$\overline{\boldsymbol{\hbar}} = \boldsymbol{\hbar} \odot \mathbf{e}_{\mathrm{ref}}$$

$$\overline{\mathbf{g}}_j = [e^{\jmath\kappa\sqrt{x_1^2+y_j^2}}, \cdots, e^{\jmath\kappa\sqrt{x_{G_x}^2+y_j^2}}]^T,$$

(1) can be formulated as a **convolution** and implemented by **FFT**

$$\tilde{E}\left(\mathbf{r}^{(:,j)}\right) = \left|\mathcal{F}_{G'_x}^{-1}\left[\mathcal{F}_{G'_x}\left[\overline{\boldsymbol{\hbar}}\right] \odot \mathcal{F}_{G'_x}\left[\overline{\mathbf{g}}_j\right]\right]_{N_{\mathrm{BS}}:G'_x-N_{\mathrm{BS}}-1}\right|.$$

Accelerate Reconstruction via FFT

- Enumerating $\tilde{E}\left(\mathbf{r}^{(i,j)}\right)$ at all possible locations can be computationally heavy
- Reconstruction formula at the (i,j) grid

$$\tilde{E}\left(\mathbf{r}^{(i,j)}\right) = \sum_{n=1}^{N_{\mathrm{BS}}} \boldsymbol{\hbar}[n]\mathbf{e}_{\mathrm{ref}}[n] \quad e^{\jmath\kappa\sqrt{\left(x_{\mathrm{BS}}^{(n)}-x_i\right)^2+y_j^2}}. \tag{1}$$

- Let

$$\overline{\boldsymbol{\hbar}} = \boldsymbol{\hbar} \odot \mathbf{e}_{\mathrm{ref}}$$

$$\overline{\mathbf{g}}_j = [e^{\jmath\kappa\sqrt{x_1^2+y_j^2}}, \cdots, e^{\jmath\kappa\sqrt{x_{G_x}^2+y_j^2}}]^T,$$

(1) can be formulated as a **convolution** and implemented by **FFT**

$$\tilde{E}\left(\mathbf{r}^{(:,j)}\right) = \left|\mathcal{F}_{G_x'}^{-1}\left[\mathcal{F}_{G_x'}\left[\overline{\boldsymbol{\hbar}}\right] \odot \mathcal{F}_{G_x'}\left[\overline{\mathbf{g}}_j\right]\right]_{N_{\mathrm{BS}}:G_x'-N_{\mathrm{BS}}-1}\right|.$$

Numerical Results: Localization

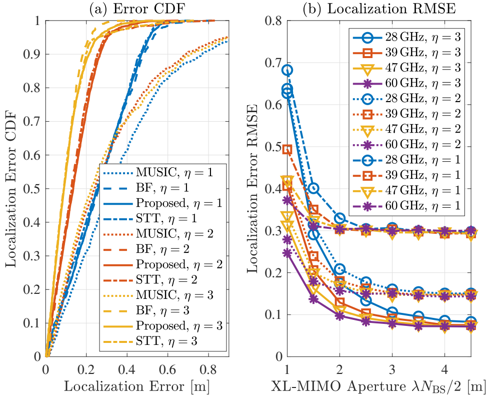

Figure 6: (a) The CDF of localization error; (b) RMSE of the localization algorithm with varying carrier frequencies and XL-MIMO aperture.

- Comparable CDFs with benchmarks
- No need for baseband sampling via ADCs
- Tens of orders of magnitude reduction in complexity

Outline

Channel Sparse Representation

- Compressive sensing

$$\min_{\tilde{\mathbf{h}}} \|\tilde{\mathbf{h}}\|_0, \qquad \text{s.t. } \|\mathbf{\Phi}\mathbf{\Psi}\tilde{\mathbf{h}} - \mathbf{y}\|_2 \leq \varepsilon,$$

  - $\mathbf{y}$: Received signal
  - $\mathbf{\Phi}$: Measurement matrix
  - $\tilde{\mathbf{h}}$: Sparse support vector to be estimated
  - $\mathbf{\Psi}$: Dictionary

- Challenges in NF channel estimation
  - Two DoFs require more codewords in $\mathbf{\Psi}$ $\Rightarrow$ Bulky dictionary
  - Higher rank NF channel $\Rightarrow$ Excessive pilot length τ

Sensing-Enhanced Channel Estimation

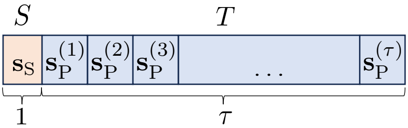

Figure 7: Proposed sensing-enhanced uplink channel estimation protocol.

- One additional slot for localization
- Localization results are utilized in channel estimation during transmission stage
- Only adding one sensing slot will significantly reduce pilot length τ and size of dictionary $\mathbf{\Psi}$

Dictionary Design

- Channel matrix $\mathbf{H}$ can be properly sparsified via its SVD $\mathbf{H} = \mathbf{U}\boldsymbol{\Sigma}\mathbf{V}^H$ $\Rightarrow \boldsymbol{\Psi} = \mathbf{V}^* \otimes \mathbf{U}$

- Consider the EVD of auto-correlation $\mathbf{R}_{\mathrm{BS}} = \mathbb{E}\left[\mathbf{H}\mathbf{H}^H\right]$
- Introducing paraxial approximation [2]

$$\mathbf{R}_{\mathrm{BS}}[n', n] \simeq \gamma_n \mathbb{1}\{n = n'\} + \frac{1}{r_0^2} \sum_{m=1}^{N_{\mathrm{UE}}} e^{-\jmath\kappa \frac{\left(x_{\mathrm{BS}}^{(n)} - x_{\mathrm{UE}}^{(m)}\right)^2 - \left(x_{\mathrm{BS}}^{(n')} - x_{\mathrm{UE}}^{(m)}\right)^2}{2\hat{y}^{(0)}}}$$

  - $\hat{y}^{(0)}$: Estimate of the UE location
  - $\gamma_n = \frac{1}{L}\sum_{\ell=1}^{L}\sum_{m}^{N_{\mathrm{UE}}} \frac{1}{\|\mathbf{r}_{\mathrm{UE}}^{(m)} - \hat{\mathbf{r}}_{\mathrm{S}}^{(\ell)}\|^2 \|\mathbf{r}_{\mathrm{BS}}^{(n)} - \hat{\mathbf{r}}_{\mathrm{S}}^{(\ell)}\|^2}$

[2] D. A. B. Miller, "Communicating with waves between volumes: Evaluating orthogonal spatial channels and limits on coupling strengths," *Appl. Opt.*, vol. 39, no. 11, pp. 1681–1699, Apr. 2000.

Dictionary Design

- Rewrite the auto-correlation as

$$\mathbf{R}_{\mathrm{BS}}[n', n] \simeq \gamma_n \mathbb{1}\{n = n'\} + e^{\jmath\kappa \frac{\left(x_{\mathrm{BS}}^{(n')}\right)^2 - \left(x_{\mathrm{BS}}^{(n)}\right)^2}{2\hat{y}^{(0)}}} \overline{\mathbf{R}}_{\mathrm{BS}}[n', n]$$

- The structure of auto-correlation suggests that the following EVD holds

$$\mathbf{R}_{\mathrm{BS}}\mathbf{u}_n = \mathbf{D}_{\mathrm{BS}}^{-1}\left(\mathbf{\Gamma} + \overline{\mathbf{R}}_{\mathrm{BS}}\right)\mathbf{D}_{\mathrm{BS}}\mathbf{u}_n = \lambda_n \mathbf{u}_n.$$

- The matrix $\overline{\mathbf{R}}_{\mathrm{BS}}[n', n]$ is a **Toeplitz Sinc** matrix

$$\overline{\mathbf{R}}_{\mathrm{BS}}[n', n] = \frac{1}{r_0^2} \sum_{m=1}^{N_{\mathrm{UE}}} e^{\jmath\kappa \frac{x_{\mathrm{UE}}^{(m)}\left(x_{\mathrm{BS}}^{(n)} - x_{\mathrm{BS}}^{(n')}\right)}{\hat{y}^{(0)}}} \propto \frac{\sin\left[2\pi W (x_{\mathrm{BS}}^{(n)} - x_{\mathrm{BS}}^{(n')})\right]}{\left(x_{\mathrm{BS}}^{(n)} - x_{\mathrm{BS}}^{(n')}\right)},$$

where $W = \kappa L_{\mathrm{R}}/(4\pi\hat{y}^{(0)})$.

Dictionary Design

- The eigenvectors of $\{\mathbf{u}_n\}_{n=1}^{N_{\rm BS}}$ of auto-correlation matrix $\overline{\mathbf{R}}_{\rm BS}[n', n]$ are known as *discrete prolate spheroidal sequence* (DPSS) or *Slepian sequence* [3] within frequency W

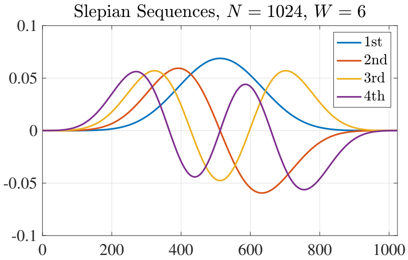

- Estimation of the auto-correlation and its EVD requires numerous samples. The **closed-form** solution here make it efficient to generate the dictionary.

[3] D. Slepian, "Estimation of signal parameters in the presence of noise," *IRE Trans. Inf. Theory*, vol. 3, no. 3, pp. 68–89, 1954.

Numerical Results: Pilot Overhead

- Near-field CE error with $I = 30$ OMP iterations

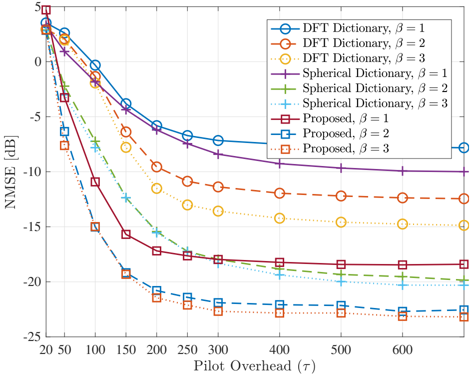

Figure 8: Performance comparison of near-field channel estimation error versus pilot length.

- To achieve a CE NMSE of -10 dB, the proposed method saves up to 85.7% of the pilot overhead when compared to the spherical dictionary [4]

[4] M. Cui and L. Dai, "Channel estimation for extremely large-scale MIMO: Far-field or near-field?" *IEEE Trans. Commun.*, vol. 70, no. 4, pp. 2663–2677, 2022

Numerical Results: Dictionary Size

- **Minimum required** dictionary size for target NMSE

Dictionaries	Baseband Samples			Dictionary Size		
	Target NMSE					
	-15 dB	-20 dB	-25 dB	-15 dB	-20 dB	-25 dB
DFT	256	358	410	2,304	4,096	4,096
Spherical [4]	205	358	N/A	1,620	4,096	N/A
Proposed	**154**	**174**	**205**	1,024+L	1,024+L	1,024+L

- A drastic reduction in baseband samples and dictionary size by up to 67% and 66%, respectively

[4] M. Cui and L. Dai, "Channel estimation for extremely large-scale MIMO: Far-field or near-field?" *IEEE Trans. Commun.*, vol. 70, no. 4, pp. 2663–2677, 2022.

Summary

- **Power measurement** works under near-field XL-MIMO
- **Sensing** results help reduce the pilot overhead and ensued baseband samples
- **Eigen-dictionary** saves storage and promote convergence

Paper Info

[J1] S. Liu, X. Yu, Z. Gao, J. Xu, D. W. K. Ng, and S. Cui, "Sensing enhanced channel estimation for near-field XL-MIMO systems," *IEEE J. Sel. Areas Commun.*, vol. 43, no. 3, pp. 628-643, Mar. 2025.

Latest update: https://arxiv.org/pdf/2403.11809

Outline

Position Reconfigurable Antenna Arrays

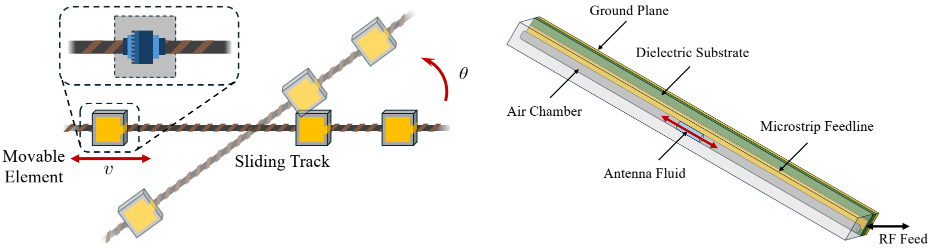

Figure 9: Implementations of position reconfigurable arrays (PRAs): Movable antennas (Left) and fluid antennas (Right).

- Antenna positions offer new design DoFs for wireless systems [5]

[5] L. Zhu, W. Ma, and R. Zhang, "Movable antennas for wireless communication: Opportunities and challenges," *IEEE Commun. Mag.*, vol. 62, no. 6, pp. 114–120, 2024.

Motivations

Limitations of current research works

- High **computational complexity**, lack of **scalability** with **massive** antennas
- Lack of system-level design **insights**
- Neglect of **near-field** effects

What we provide:

- Acceptable complexity, scalable for **massive/XL-MIMO**
- Provide **closed-form solutions** with physical insights
- Suitable for **near-field** scenarios

Motivations

Limitations of current research works

- High **computational complexity**, lack of **scalability** with **massive** antennas
- Lack of system-level design **insights**
- Neglect of **near-field** effects

What we provide:

- Acceptable complexity, scalable for **massive/XL-MIMO**
- Provide **closed-form solutions** with physical insights
- Suitable for **near-field** scenarios

System Model

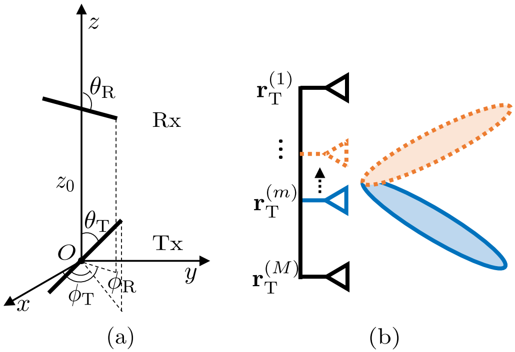

Figure 10: Near-field scenario and movable antennas.

- Downlink point-to-point with dominant LoS channel
- M movable antennas at BS (Tx), N fixed antennas at UE (Rx)

Outline

Antenna Position Function

- Antennas move freely on a linear array with coordinate

$$\begin{cases} x_{\mathrm{T}}^{(m)} & = \frac{A_{\mathrm{T}}}{2} f(m) \sin\theta_{\mathrm{T}} \cos\phi_{\mathrm{T}} \\ y_{\mathrm{T}}^{(m)} & = \frac{A_{\mathrm{T}}}{2} f(m) \sin\theta_{\mathrm{T}} \sin\phi_{\mathrm{T}}, \quad \forall m \in \mathcal{M}, \\ z_{\mathrm{T}}^{(m)} & = \frac{A_{\mathrm{T}}}{2} f(m) \cos\theta_{\mathrm{T}} \end{cases}$$

  where
  - $\mathcal{M} = \{m \in \mathbb{Z} \mid 1 \leq m \leq M\}$
  - $A_{\mathrm{T}} = (M-1)d$, aperture.
- $p = f(m) \in [-1, 1]$ is the continuous **antenna position function** (APF).
- For ULA case, APF is given by

$$f^{\mathrm{uni}}(m) = \frac{2}{M-1}\left(m - \frac{M+1}{2}\right).$$

Antenna Density Function

- The number of antenna elements within unit length

$$w(p) = \lim_{\Delta p \to 0} \frac{f^{-1}(p + \Delta p) - f^{-1}(p)}{\Delta p} = \frac{\mathrm{d}}{\mathrm{d}p} f^{-1}(p),$$

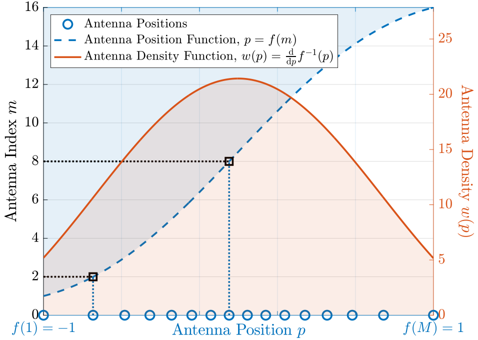

Figure 11: APF $p = f(m)$ (in blue) and ADF $w(p)$ (in orange).

Problem Formulation

- Find optimal $w(p)$ to maximize the achievable rate *functional*

$$C_w = \log_2 \det \left(\mathbf{I} + \frac{P_{\mathrm{T}}}{M\sigma_{\mathrm{n}}^2} \mathbf{H}_w \mathbf{H}_w^H \right)$$

- We shall study the property of Toeplitz matrix

$$\mathbf{T}_N = \mathbf{I} + \frac{\rho}{M} \mathbf{H}_w \mathbf{H}_w^H \triangleq \mathbf{I} + \rho \overline{\mathbf{K}}_w$$

- **Goal:** To optimize ADF $w(p)$ that maximizes $\log \det_2(\mathbf{T}_N)$

Useful Preliminaries

Definition 1: Generating Function of Toeplitz Matrix

Let $s(\theta)$ be a real smooth and non-vanishing function defined on unit circle with Fourier coefficients

$$c_k = \frac{1}{2\pi}\int_0^{2\pi} s(\theta)e^{-\jmath k\theta}\,\mathrm{d}\theta, \quad k \in \mathbb{Z}.$$

If a Toeplitz matrix $\mathbf{T}_N$ admits the form as

$$\mathbf{T}_N = \begin{bmatrix} c_0 & c_{-1} & c_{-2} & \cdots & c_{1-N} \\ c_1 & c_0 & c_{-1} & \cdots & c_{2-N} \\ \vdots & \vdots & \vdots & \ddots & \vdots \\ c_{N-1} & c_{N-2} & c_{N-3} & \cdots & c_0 \end{bmatrix},$$

then $s(\theta)$ is called the **generating function** of $\mathbf{T}_N$.

ADF and Generating function

- A Toeplitz matrix $\mathbf{T}_N$ is associated with its generating function $s(\theta)$
- We proved that the generating function of $\mathbf{T}_N = \mathbf{I} + \rho\overline{\mathbf{K}}_w$ is closely related to the ADF $w(p)$, given by

$$s(\theta) = 1 + \frac{2\pi\rho}{\beta z_0^2 \left(1 + \tau\left(\frac{\theta}{\beta}\right)\right)^2} w\left(\frac{\theta}{\beta}\right),$$

  where $\beta = \frac{\kappa A_{\mathrm{T}} A_{\mathrm{R}} \sin\theta_{\mathrm{T}} \sin\theta_{\mathrm{R}} \cos(\phi_{\mathrm{T}} - \phi_{\mathrm{R}})}{z_0(N-1)}$ and $\tau = \frac{A_{\mathrm{T}}}{2z_0}\cos\theta_{\mathrm{T}}$ are two antenna geometry-related parameters.
- **Goal transfer:** Optimize $s(\theta)$ to maximize $\log\det_2(\mathbf{T}_N)$

Optimal ADF

Fisher-Hartwig Theorem [6], [7]

The optimal generating function

$$s^\star(\theta) \propto |1-\cos(\theta-\beta)|^\alpha \, |1-\cos(\theta+\beta)|^\alpha, \quad -\frac{1}{2} < \alpha < 0$$

- Substituting Maclaurin series $1-\cos\theta = \theta^2/2 + \mathcal{O}(\theta^2)$

$$s^\star(\theta) \propto \frac{1}{\left(\beta^2-\theta^2\right)^{-2\alpha}} \;\Rightarrow\; w^\star(p) = \left(\frac{\gamma_\alpha}{\left(1-p^2\right)^{-2\alpha}} - \frac{\beta z_0^2}{2\pi\rho}\right)(1+\tau p)^2$$

[6] M. E. Fisher and R. E. Hartwig, "Toeplitz determinants: Some applications, theorems, and conjectures," in *Advances in Chemical Physics*. John Wiley & Sons, Ltd, 1969, pp. 333–353.
[7] A. Lenard, "Some remarks on large Toeplitz determinants.," *Pacific Journal of Mathematics*, vol. 42, no. 1, pp. 137–145, 1972.

A Glimpse of ADF

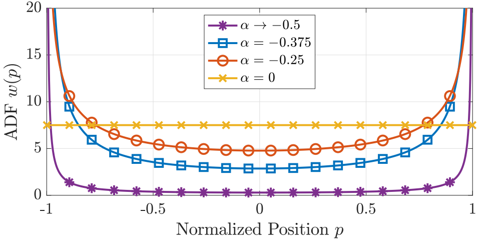

- $\alpha = 0 \Leftrightarrow$ ULA
- "U"-shape: a denser deployment of antenna elements at the edges of the array efficiently captures the higher spatial frequency of spherical waves at the array periphery

Log-Det in the Rate Functional

Fisher-Hartwig Theorem [6], [7]

$$\begin{aligned} C_w &= \log\det\left(\mathbf{I} + \rho\overline{\mathbf{K}}_w\right) \\ &= \log N \sum_{r=1}^{2} \alpha_r^2 + \sum_{r=1}^{2} \frac{\mathrm{BG}^2(1+\alpha_r)}{\mathrm{BG}(1+2\alpha_r)} + (2 - 2\cos 2\beta)^{-\alpha_1\alpha_2} + \textbf{const}, \end{aligned}$$

where $BG(\cdot)$ denotes the Barnes G-function.

- When $N \to \infty$, $\frac{\mathrm{d}C_w}{\mathrm{d}\alpha_i} < 0$
- The smaller the α is, the denser antenna deployment at two edges, and the higher spectral efficiency achieved

[6] M. E. Fisher and R. E. Hartwig, "Toeplitz determinants: Some applications, theorems, and conjectures," in *Advances in Chemical Physics*. John Wiley & Sons, Ltd, 1969, pp. 333–353.
[7] A. Lenard, "Some remarks on large Toeplitz determinants.," *Pacific Journal of Mathematics*, vol. 42, no. 1, pp. 137–145, 1972.

Discretization

- $M = 16$ Antenna positions on a normalized linear array

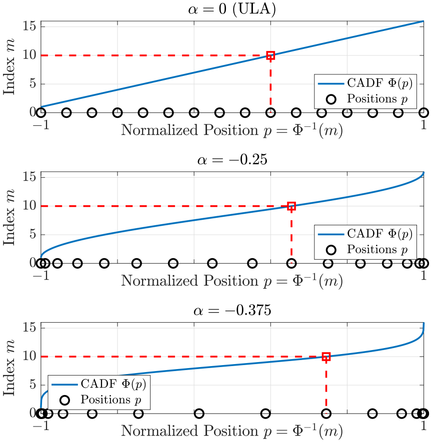

- $\alpha \uparrow \Rightarrow$ 1) $C_w \uparrow$ 👍
  2) Antenna spacing $\downarrow$ 👎

[8] S. Liu and X. Yu, "Low-complexity near-field localization with XL-MIMO sectored uniform circular arrays," in *Proc. IEEE Global Commun. Conf. (GLOBECOM)*, 2024, pp. 4756–4761

Discretization

- $M = 16$ Antenna positions on a normalized linear array

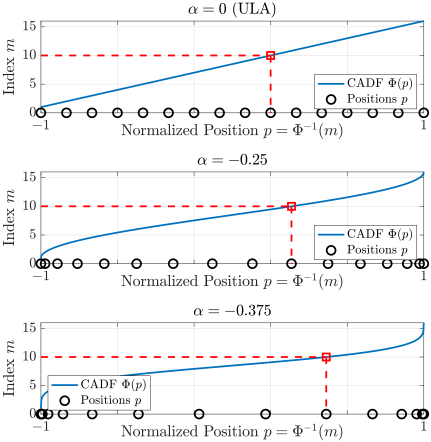

- $\alpha \uparrow \Rightarrow$ 1) $C_w \uparrow$
  2) Antenna spacing $\downarrow$
- $\alpha = -0.25 \leftrightarrow$ uniform circular array (UCA) [8]

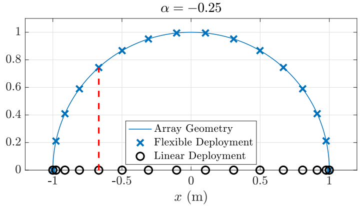

[8] S. Liu and X. Yu, "Low-complexity near-field localization with XL-MIMO sectored uniform circular arrays," in *Proc. IEEE Global Commun. Conf. (GLOBECOM)*, 2024, pp. 4756–4761

Numerical Results

- Antenna positions have significant effect on achievable rate
- By simply adopting UCA, achievable rate can be improved

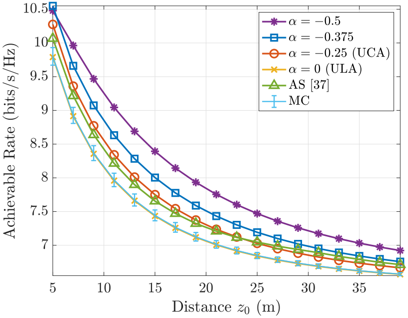

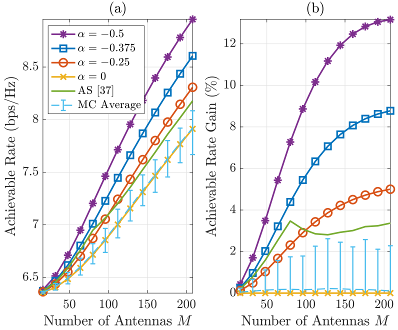

- Up to 13% performance gain by closed-form solution

Numerical Results

- Optimal ADF for different incident directions Link

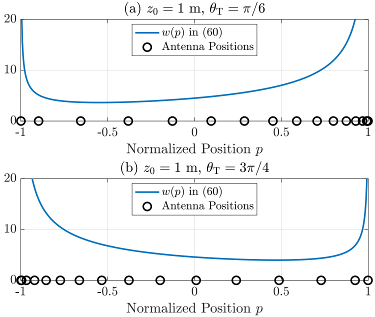

- Antennas tend to cluster towards the incident direction
- Higher wavefront curvature of the EM wave at the near end of the array
- Higher sampling rate at the near end in the near-field region

Summary

- Antenna positions can affect the intrinsic structure of channel matrix
- **Closed-form** ADF can be obtained to maximize the achievable rate
- **Edge antenna density** has a significant effect on capacity (up to 13%)

Paper Info

[J2] S. Liu, X. Yu, J. Xu, and R. Zhang, "Near-field communication with massive movable antennas: A functional perspective," *under major revision.*

- However, the discretization process may result in some performance loss

Summary

- Antenna positions can affect the intrinsic structure of channel matrix
- **Closed-form** ADF can be obtained to maximize the achievable rate
- **Edge antenna density** has a significant effect on capacity (up to 13%)

Paper Info

[J2] S. Liu, X. Yu, J. Xu, and R. Zhang, "Near-field communication with massive movable antennas: A functional perspective," *under major revision.*

- However, the discretization process may result in some performance loss

Outline

Analysis of Spectral Efficiency

- Under a typical near-field communication setting

$$
\begin{aligned}
R_{\mathbf{x}} &= \log_2 \det\left(\mathbf{I}_N + \frac{\rho}{M}\mathbf{H}_{\mathbf{x}}\mathbf{H}_{\mathbf{x}}^H\right) \\
&\simeq \log_2 \det\left(\mathbf{D}_{\mathrm{T}}\mathbf{D}_{\mathrm{T}}^H\right) + \log_2 \det\left(\left(\underline{\mathbf{V}}_{\mathrm{T}}\right)^H \underline{\mathbf{V}}_{\mathrm{T}}\right) + \text{const},
\end{aligned}
$$

where $\mathbf{x} = \left[x_{\mathrm{BS}}^{(1)}, x_{\mathrm{BS}}^{(2)}, \cdots, x_{\mathrm{BS}}^{(M)}\right]$ are antenna positions,

$$
\mathbf{D}_{\mathrm{T}} = \mathrm{diag}\left(\left[\frac{e^{\jmath\kappa r_1}}{r_1}, \frac{e^{\jmath\kappa r_2}}{r_2}, \cdots, \frac{e^{\jmath\kappa r_M}}{r_M}\right]\right) \quad \Leftarrow \text{Diagonal}
$$

$$
\mathbf{V}_{\mathrm{T}} = \begin{bmatrix} 1 & \sin\left(\varphi_1 - \theta_{\mathrm{UE}}\right) & \sin^2\left(\varphi_1 - \theta_{\mathrm{UE}}\right) & \cdots \\ 1 & \sin\left(\varphi_2 - \theta_{\mathrm{UE}}\right) & \sin^2\left(\varphi_2 - \theta_{\mathrm{UE}}\right) & \cdots \\ \vdots & \vdots & \vdots & \cdots \\ 1 & \sin\left(\varphi_M - \theta_{\mathrm{UE}}\right) & \sin^2\left(\varphi_M - \theta_{\mathrm{UE}}\right) & \cdots \end{bmatrix} \quad \Leftarrow \text{Vandermonde}
$$

Problem Formulation

- ***Weighted Fekete problem*** [9]

$$\begin{aligned} \max_{\mathbf{s}} \quad & 2 \sum_{1 \le i < j \le M} \log_2 (s_j - s_i) + \sum_{m=1}^{M} \log_2 \left(1 - \tilde{s}_m^2\right) \\ \text{s.t.} \quad & s_{\min} = s_1 < s_2 < \cdots < s_M = s_{\max}, \end{aligned}$$

where $s_m = \sin(\varphi_m - \theta_{\mathrm{UE}})$ and $\tilde{s}_m = \sin \varphi_m = \sin(\arcsin s_m + \theta_{\mathrm{UE}})$

- Proved to be *convex*
- Physical insights

[9] E. B. Saff and V. Totik, *Logarithmic Potentials with External Fields* (Grundlehren der mathematischen Wissenschaften), Second. Cham, Switzerland: Springer, 1997, vol. 316, ISBN: 978-3-031-65133-5.

Weighted Fekete Problem

- Weighted Fekete problem seeks the optimal distribution of M charges achieves a balance between **internal** interaction mutual repulsion and **external** influence

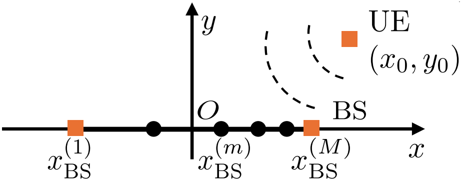

- Mutual coupling among antennas corresponds to the **internal** interaction
- The field induced by the UE serves as the **external** field
- Positions of $M-2$ movable antennas have to be delicately optimized to obtain a state of equilibrium between these two forces

Greedy Position Selection

- To relax the computational complexity of convex optimization algorithms ($\sim \mathcal{O}\left(M^3\right)$), we introduce greedy antenna selection
- Select the **next** antenna position that maximize the **local optimal** rate
- For the m-th antenna, define the **local objective** (c.f. Page 48)

$$J(s) = 2\sum_{i=1}^{m-1} \log_2 |s_i^\star - s| + \log_2\left(1 - \sin^2\left(\arcsin s + \theta_{\mathrm{UE}}\right)\right)$$

- Do

$$\boxed{\text{Update Feasible Region } \mathcal{S} \quad \rightleftharpoons \quad \text{Find } s_m^\star = \arg\max_{s\in\mathcal{S}}\left(J(s)\right)}$$

Until all $M-2$ antenna elements are assigned

Greedy Position Selection

- To relax the computational complexity of convex optimization algorithms ($\sim \mathcal{O}\left(M^3\right)$), we introduce greedy antenna selection
- Select the **next** antenna position that maximize the **local optimal** rate
- For the m-th antenna, define the **local objective** (c.f. Page 48)

$$J(s) = 2\sum_{i=1}^{m-1} \log_2 |s_i^\star - s| + \log_2\left(1 - \sin^2\left(\arcsin s + \theta_{\mathrm{UE}}\right)\right)$$

- Do

$$\boxed{\text{Update Feasible Region } \mathcal{S} \quad \rightleftharpoons \quad \text{Find } s_m^\star = \arg\max_{s\in\mathcal{S}} \left(J(s)\right)}$$

Until all $M-2$ antenna elements are assigned

Greedy Position Selection

- To relax the computational complexity of convex optimization algorithms ($\sim \mathcal{O}\left(M^3\right)$), we introduce greedy antenna selection
- Select the **next** antenna position that maximize the **local optimal** rate
- For the m-th antenna, define the **local objective** (c.f. Page 48)

$$J(s) = 2\sum_{i=1}^{m-1} \log_2 |s_i^\star - s| + \log_2 \left(1 - \sin^2\left(\arcsin s + \theta_{\mathrm{UE}}\right)\right)$$

- Do

$$\boxed{\text{Update Feasible Region } \mathcal{S} \quad \rightleftharpoons \quad \text{Find } s_m^\star = \arg\max_{s\in\mathcal{S}} \left(J(s)\right)}$$

Until all $M-2$ antenna elements are assigned

Greedy Position Selection

- (Left) Achieve higher rates with limited performance degradation compared to CVX.
- (Right) Greedy positions show distributional conformity with CVX results.

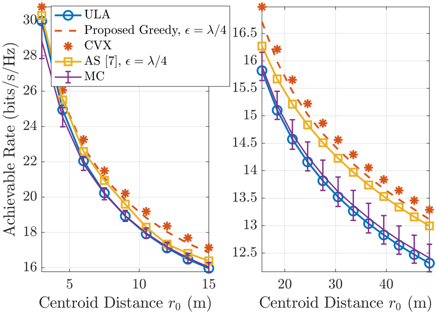

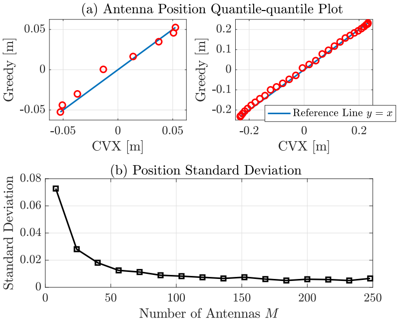

Summary

- The movable antenna placement problem in the near field is closely related to the classic potential energy equilibrium theory
- Efficient greedy algorithm can be applied to antenna positioning to maximize the achievable rate

Paper Info

[C1] S. Liu and X. Yu, "Near-field line-of-sight communication with massive movable antennas," submitted to *IEEE Int. Conf. Commun. (ICC)*, Glasgow, Scotland, UK, May 2026.

Outline

Conclusion

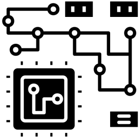

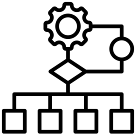

	Hardware	Algorithm

Conclusion

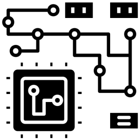

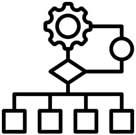

	Hardware	**Algorithm**
Localization	Power sensors	Back projection
Channel estimation		DPSS dictionary

Conclusion

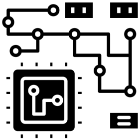

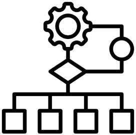

	Hardware	**Algorithm**
Localization	Power sensors	Back projection
Channel estimation		DPSS dictionary
Communication	Movable antennas	Closed-form U-shape ADF
		Weighted Fekete Problem

Conclusion

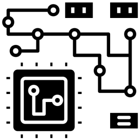

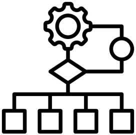

	Hardware	**Algorithm**
Localization	Power sensors	Back projection
Channel estimation		DPSS dictionary
Communication	Movable antennas	Closed-form U-shape ADF
		Weighted Fekete Problem

- Tailored hardware and low-complexity algorithms for near-field S&C

[1] A. Fenn, "Evaluation of adaptive phased array antenna, far-field nulling performance in the near-field region," *IEEE Trans. Antennas Propag.*, vol. 38, no. 2, pp. 173–185, 1990.

[2] D. A. B. Miller, "Communicating with waves between volumes: Evaluating orthogonal spatial channels and limits on coupling strengths," *Appl. Opt.*, vol. 39, no. 11, pp. 1681–1699, Apr. 2000.

[3] D. Slepian, "Estimation of signal parameters in the presence of noise," *IRE Trans. Inf. Theory*, vol. 3, no. 3, pp. 68–89, 1954.

[4] M. Cui and L. Dai, "Channel estimation for extremely large-scale MIMO: Far-field or near-field?" *IEEE Trans. Commun.*, vol. 70, no. 4, pp. 2663–2677, 2022.

[5] L. Zhu, W. Ma, and R. Zhang, "Movable antennas for wireless communication: Opportunities and challenges," *IEEE Commun. Mag.*, vol. 62, no. 6, pp. 114–120, 2024.

[6] M. E. Fisher and R. E. Hartwig, "Toeplitz determinants: Some applications, theorems, and conjectures," in *Advances in Chemical Physics*. John Wiley & Sons, Ltd, 1969, pp. 333–353.

[7] A. Lenard, "Some remarks on large Toeplitz determinants.," *Pacific Journal of Mathematics*, vol. 42, no. 1, pp. 137–145, 1972.

[8] S. Liu and X. Yu, "Low-complexity near-field localization with XL-MIMO sectored uniform circular arrays," in *Proc. IEEE Global Commun. Conf. (GLOBECOM)*, 2024, pp. 4756–4761.

[9] E. B. Saff and V. Totik, *Logarithmic Potentials with External Fields* (Grundlehren der mathematischen Wissenschaften), Second. Cham, Switzerland: Springer, 1997, vol. 316, ISBN: 978-3-031-65133-5.

[10] M. Desai and W. Jenkins, "Convolution backprojection image reconstruction for spotlight mode synthetic aperture radar," *IEEE Trans. Image Process.*, vol. 1, no. 4, pp. 505–517, 1992.

[11] S. Li, S. Wang, M. G. Amin, and G. Zhao, "Efficient near-field imaging using cylindrical MIMO arrays," *IEEE Trans. Aerosp. Electron. Syst.*, vol. 57, no. 6, pp. 3648–3660, 2021.

[12] D. Gabor, "Microscopy by Reconstructed Wave-Fronts," *Proceedings of the Royal Society of London Series A*, vol. 197, no. 1051, pp. 454–487, 1949.

[13] D. Sheen, D. McMakin, and T. Hall, "Three-dimensional millimeter-wave imaging for concealed weapon detection," *IEEE Trans. Microw. Theory Techn.*, vol. 49, no. 9, pp. 1581–1592, Sep. 2001.

[14] J. Liu, T. Su, B. Wu, and H. Lv, "Holographic design of leaky-wave antenna with gain controlled four beams," *Microw. Opt. Technol. Lett.*, vol. 61, no. 3, pp. 638–643, 2019.

Thanks for your attention!
Q & A

Contact: alex.yu@cityu.edu.hk
sc.liu@my.cityu.edu.hk

Slides & Codes: `https://github.com/scliubit/sensing-ce-xlmimo`